Electrical modulation of static and dynamic spectroscopic properties of coupled nanoscale GaSe quantum dot assemblies

Y. K. Verma, R. H. Inman, C. G. L. Ferri, H. Mirafzal, S. N. Ghosh, D. F. Kelley, L. S. Hirst, and S. Ghosh*
School of Natural Sciences, University of California, Merced, California 95343, USA

W. C. Chin
School of Engineering, University of California, Merced, California 95343, USA

(Received 7 June 2010; revised manuscript received 30 August 2010; published 15 October 2010)

We demonstrate the formation and spatial modulation of strongly coupled gallium selenide quantum dot (QD) nanoassemblies suspended in a nematic liquid-crystal (NLC) matrix at room temperature. Using static and dynamic optical techniques we show that the coupled QDs aggregate with a well-defined directionality commensurate with the NLC director axis. This results in highly anisotropic spectral properties of the QD assembly. The spatial orientation of the aggregates is selectively controlled *in situ* by the application of in-plane electric fields. The strong interdot coupling further increases the excitonic recombination rate which is both direction and electric field dependent. This electrical modulation, a noninvasive process, could potentially be an important functionality for the design and creation of building blocks for novel optoelectronic devices.

DOI: 10.1103/PhysRevB.82.165428 PACS number(s): 73.21.La, 78.55.−m, 78.47.jd

Semiconducting quantum dots (QDs) are characterized by a number of unique properties that originate from the quantum confinement effect of their reduced dimensionality. These include discrete density of states, ease of generating single excitations per QD and long coherence times. Communication between QDs, brought about by coupling of these discrete energy states, result in collective behavior that can be harnessed for a multitude of applications.[1,2] For example, coherent coupling of their discrete electronic or excitonic states is the central theme in many quantum computation schemes[3,4] while incoherent long-range energy-transfer mechanisms in close-packed assemblies can find applications in photovoltaic devices.[5,6] Chemically synthesized QDs—with high quantum yield and room-temperature spin coherence[7,8]—are excellent candidates for these platforms. However, the ability to form large, organized arrays of these nanoparticles, and the capability to manipulate and influence the interparticle interactions, while essential for practical applications in quantum or classical devices, has proven to be experimentally difficult. Here, we present a means of forming postsynthesis aggregates of strongly coupled GaSe QDs by suspending them in a matrix of nematic liquid crystal (NLC) molecules. The spectral signatures suggest that the interdot coupling is stronger than that typically observed in other chemically synthesized QDs (Ref. 9) and that the QDs aggregate along preferred directions due to the presence of the NLC molecules. The spatial orientation of these aggregates and the exciton recombination lifetime is altered *in situ* by the application of in-plane electric fields.

Chemically synthesized III-VI GaSe QDs differ from most other semiconductor nanoparticles in their unique disklike shape [Fig. 1(A), insets]. It originates from the intrinsic layered bulk crystal structure where each layer consists of four atomic sheets of Se-Ga-Ga-Se and spans about 0.8 nm.[10,11] The QDs are a single-layer thick with diameters ranging from 2.5 to 12 nm, resulting in the formation of a nanodisk. GaSe QDs are synthesized using variation in the methods as reported in previous publications.[12–14] The photoluminescence (PL) spectrum of a solution of QDs (median diameter ~5.5 nm) in toluene is shown in Fig. 1(A). The observed peak at 478 nm (2.61 eV) is blueshifted with respect to the bulk GaSe band gap of 2.1 eV.[11] This is a result of strong quantum confinement occurring along all three dimensions. Previous studies have shown that about 80% of this confinement is due to the single-layer nature of the particles and the remaining due to the finite diameter of the

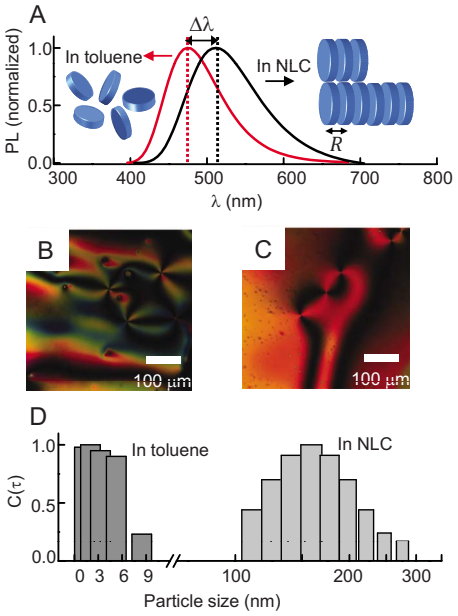

FIG. 1. (Color online) (a) Comparison of normalized PL spectra of QDs in toluene and in NLC matrix. The emission for the latter is redshifted by $\Delta\lambda = 37$ nm. The schematics represent the arrangement of QDs for both these cases. Schlieren texture of the nematic phase imaged with polarization optical microscopy for (b) unaligned pure NLC, (c) unaligned NLC with QDs 30:1 by volume confirming the presence of the nematic phase in the mixture. (d) Particle size distribution from DLS characterization of QDs in toluene (dark gray) and in NLC (light gray).

nanodisk.[14] GaSe QDs are known to aggregate at room temperature in solution, resulting in a slight redshift of approximately 12 nm of their emission spectrum.[12] These aggregates are analogous to the J aggregates of organic dyes[15,16] and chromophores in photosynthetic systems.[17,18] The extent of the redshift is determined by the magnitude of the interparticle dipolar coupling, which depends on two factors: the interparticle separation and the extent of disorder in the aggregate. The interparticle separation can be controlled chemically since adjacent particles are held apart by the steric constraints imposed by the ligands on the particle edges. Replacing bulkier ligands (such as commonly used trioctyl phosphine and trioctyl phosphine oxide) with far less bulky alkyl aldehydes is one way to accomplish this in solution.[19] However, the extent of disorder in the aggregates is impossible to control without the aid of external agents. In an effort to reduce this disorder and increase the interparticle coupling we suspend the QDs in 4 cyano-4′ pentyl biphenyl (commonly known as 5CB, purchased from Sigma-Aldrich), which forms an NLC phase at room temperature.

For preparing the QD-NLC mixture we use a 1:25 volume ratio of QD solution to 5CB and thermally cycle the mixture repeatedly through the nematic-isotropic transition of 5CB (40 °C) for 1 h. Using polarization microscopy we ensure that the sample is well mixed and that the liquid crystal retains its nematic phase [Figs. 1(B) and 1(C)]. Through a systematic study we find that a uniform nematic phase is supported for up to 10% QD volume in 5CB. The peak of the QD-NLC emission spectrum is centered at 515 nm [Fig. 1(A)], redshifted by 37 nm from the corresponding spectrum in toluene. This 0.184 eV shift is comparable to that previously observed in smectic-A liquid crystals[20] and almost fivefold greater than the shifts observed in close-packed "artificial solids" of colloidal CdSe QDs.[9,21] That this interdot coupling is stronger in GaSe QDs can be understood by recalling that dipole interaction energy scales as $1/R^3$, R being the interdot separation. The disk geometry could allow GaSe QDs to stack very closely together (unlike more symmetric QDs) and one could envision a scenario as shown in Fig. 1(A) (right inset) where $R \sim 1$ nm. To verify if the QDs do assemble into aggregates as suggested, we obtain an estimate of the size of these assemblies from dynamic light scattering (DLS) measurements. For these measurements, the scattering cells are positioned in the goniometer of a Brookhaven laser spectrometer (BI-200SM, Brookhaven Instruments, Holtsville, NY, USA). Particle size is monitored by analyzing the scattering fluctuations detected at 45° scattering angle. Calibration of the DLS size measurements is conducted using standard suspensions of polystyrene nanoparticles (Bangs Laboratory, Fishers, IN, USA). As seen in Fig. 1(D), the QD solution in toluene consists primarily of monomers and its DLS study exhibits a size distribution in the range 1–9 nm. But when suspended in the NLC, the size of the particles is on the order of hundreds of nanometers, indicating aggregation. From the ratio of hydrodynamic radii, we conclude that in the NLC the QDs form clusters with a membership of 15–60 QDs in each.

Next, we investigate the optical properties of these aggregates using spatially and polarization-resolved PL spectroscopy. The PL measurements are done using a custom-built

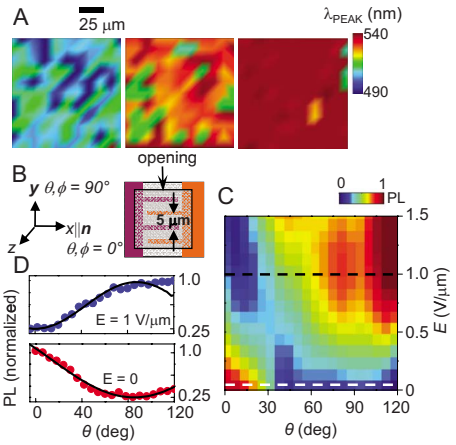

FIG. 2. (Color online) (a) (Left) Spatially resolved PL map of the QD-NLC sample showing emission in the range of 500–515 nm when the NLC is unaligned. (Center) Emission from the same sample redshifts to 520–530 nm when the NLC has a well-defined director axis **n** (coordinate system shown in B) but no applied E. (Right) A scan of the same area at $E=0.8$ V/μm with $E \| \mathbf{n}$ showing further redshift. (b) (Left) Reference coordinate system used in the text. The director **n** is identified as the x axis while the z axis is the optical axis showing the direction of the excitation/collection beams. (Right) A schematic of the cell. The interdigitated electrodes allow an application of $E \perp \mathbf{n}$ along the y axis. Cells with electrodes without the interdigitated extensions are used for applying E along **n**. (c) Normalized PL intensity as functions of applied E and incident polarization angle θ for the QD-NLC sample where $E \perp \mathbf{n}$. (d) Line cuts of (c) at different values of E (dashed lines), showing maximum emission intensity occurring at different θ with varying electric field. Lines are fits (see text).

scanning confocal microscopy setup. The scanning system uses a 100× objective to attain optical resolution of about 600 nm. For the static PL a cw laser tuned to 410 nm is used as the excitation source. The PL is collected through the 100 μm aperture of a fiber and dispersed through a 300 mm spectrometer onto a thermoelectrically cooled charge-coupled device with a spectral resolution of 0.8 nm. This system allows us to create two-dimensional emission maps of the QD emission, as shown in Fig. 2(A), elucidating the localized spatial distribution and orientation of the nanostructures. We use specialized glass cells to house the samples. These cells have an optical path length of 4 μm with indium-tin oxide (ITO) electrodes patterned on the inner surfaces which apply in-plane electric fields along desired directions. A thin coating of rubbed polyimide film on the inner surfaces define a zero-field alignment direction. We use the convention of notifying the director axis (**n**) of the nematic phase as the x axis [Fig. 2(B), left]. Figure 2(A) shows scanning PL maps of samples where we plot the peak emission wavelength λ_{PEAK} over a 100×100 μm^2 area. On the left, a sample of QDs in NLC, placed in a cell with no defined director axis, demonstrates moderate interdot coupling with emission in the range 500–515 nm. At the center is the same mixture in a similar cell, one with a defined **n** but no applied electric field ($E=0$). The emission is in the range 520–530 nm over most of the scanned area. The sample shown at the right is the same mixture but with E

$=0.8$ V/μm, applied along the x axis ($\|\mathbf{n}$). In this case, the emission is redshifted to 540 nm. This is a shift of almost 60 nm from the isolated QD emission at 478 nm. Polarization analysis of these maps shows that while the emission from a QD-toluene sample is isotropic, the absorption and emission are strongly polarized along the x axis for the QD-NLC samples shown in Fig. 2(A) (center and right). This polarization can be quantified in terms of the emission intensity as a function of the angle between the polarization of the emitted light and the x axis. Specifically, we define the polarization as $P=(I_{\|}-I_{\perp})/(I_{\|}+I_{\perp})$, where $I_{\|}$ and $I_{\perp}$ are the spectrally integrated intensities with the emission collected parallel and perpendicular to the director axis, respectively. In the case of the QD-NLC samples, $P=0.62$ for the sample mapped in Fig. 2(A) (center) with $E=0$. Since in an individual GaSe QD the lowest energy transition is polarized almost completely along the out-of-plane axis of the disk, this result indicates that when incorporated into the liquid crystal matrix, the GaSe nanoparticles are spatially aligned in the NLC environment. Alignment facilitates the formation of one-dimensional aggregates, with the QDs stacking as depicted in the schematic in Fig. 1(A), aligned along the NLC director axis. The driving force for this alignment is the reduction in the strain energy in the NLC. However, the QD alignment shows spatial inhomogeneity demarcated by regions of different spectral shifts. This is attributed to the NLC director axis not being perfectly unidirectional throughout the sample. The latter is exhibited in Figs. 1(B) and 1(C) in the form of domains of varying color and intensity. This "patchiness" persists, until, on the application of the electric field along the director axis the alignment in the NLC is maximally uniform and so is the magnitude of the strain energy induced by the remaining randomly oriented QDs. As a result, the structural disorder of the QD aggregates is further reduced and exhibited in the form of both P increasing to 0.74 at $E=0.8$ V/μm and the nonuniformity of the spectral emission decreasing. Additionally, the average interparticle coupling is also strengthened with E, which is consistent with the large spectroscopic shift observed in Fig. 2(A) (right).

In addition to the above effect of inducing better order in the ensemble, we demonstrate additional control of the aggregate polarization with E. We alter the directionality of the aggregate alignment by the application of an in-plane E perpendicular to $\mathbf{n}$, using a cell sketched in Fig. 2(B) (right) where the back surface has interdigitated ITO electrodes 5 μm apart. We use linearly polarized excitation with the capability of electronically varying the angle of polarization θ continuously using a LC-based variable wave plate, where $\theta=0°$ designates incident excitation polarized along x axis ($\perp E, \| n$) and $\theta=90°$ when polarized along y axis ($\|E$). Figure 2(B) is a plot of the spectrally integrated, normalized PL intensity as a function of θ and E. At $E=0$, the emission has a maximum at $\theta=0°$. The emission intensity can be fit to the functional form $I(\theta)=I_o \cos^2 \theta+$constant, as would be expected for aligned particles, and the angular dependence of the intensity is shown in Fig. 2(C) (bottom). The angular dependence of $I(\theta)$ changes with increasing E, until at $E=1$ V/μm the emission maximum occurs at $\theta=90°$ [Fig. 2(C), top]. At $E=0$, the NLC molecules align parallel to the rubbing direction in the cell but a nonzero E reorients them to align parallel to the field direction, along the y axis. Theoretical calculations and experimental observations show that the threshold electric field for this response lies in the range 0.69–0.72 V/μm for the NLC used. Therefore, at $E=1$ V/μm a large portion of the NLC molecules have realigned along E.

Modulation of the intensity of emitters embedded in an LC matrix is almost an expected effect. It is the basis of LC-based displays where the birefringence of NLCs is electrically manipulated to impart a controlled phase shift to light traversing the medium. Therefore, we perform a control measurement to develop a qualitative distinction between the contributions of the birefringence of the NLCs and of the emission of coupled QD aggregates to the optical anisotropy. The GaSe QDs are replaced by commercially acquired CdSe/ZnS core-shell QDs in the NLC matrix. These QDs have a CdSe core of 1.2 nm diameter but the ZnS shell and additional ligands make their interparticle separation effectively larger (~6 nm). The CdSe/ZnS QDs in NLC show two distinct differences from the GaSe-NLC sample. There are no large interdot interaction-induced spectral shifts and the emission is largely isotropic with variations in θ and E. Therefore, we conclude that (a) the optical effects observed in the GaSe-NLC matrix is due to the anisotropic properties of the GaSe QDs, rather than the birefringence of the NLC and (b) the angular variation in emission polarization can only be explained if the coupled GaSe QD structures are isomorphic to the reoriented NLC molecules and follow their spatial directionality.

The electrical modulation is not limited to the static properties of the QD nanoassemblies. For time-resolved measurements we use a time-correlated single-photon counting system (TCSPC) from PicoQuant (PicoHarp 300) with a temporal resolution of 28 ps after deconvolution of the instrument response function. The exciting laser for the TCSPC measurements is a mode-locked, tunable Ti:Sapphire with a pulse width of 150 fs and a repetition rate of 76 MHz. It is tuned to 820 nm and its output frequency doubled with a Barium beta-Borate crystal to achieve pulsed excitation at 410 nm. The excitonic recombination rate in isolated QDs is a sum of the radiative and nonradiative rates: $1/\tau_{\mathrm{QD}}=1/\tau_r+1/\tau_{nr}$. In ensembles of coupled QDs the interdot interactions introduce nonradiative channels of relaxation in the form of extra recombination sites. This dramatically reduces the excited state lifetime and the total recombination rate is modified to: $1/\tau_{CQD}=1/\tau_r+1/\tau_{nr}+1/\tau_{ET}$, where τ_{ET} is the interdot energy-transfer time. The decreased lifetime can be seen in the emission decay kinetics, shown in Fig. 3(A) which shows that the emission decay time for the QDs in NLC is indeed considerably faster than in the case of the QDs in toluene. The QDs in solution have a recombination time of $\tau_{\mathrm{QD}}=3.8$ ns while the QD-NLC sample ($E=0$) has a reduced lifetime of $\tau_{CQD}=650$ ps. Figure 3(B) shows that this decay time also depends on the magnitude of the applied electric field and the direction of excitation/emission. The PL is analyzed by a linear polarizer after collection, where we define the collection angle ϕ to be commensurate with excitation angle θ [Fig. 2(B), left]. Emission along $\mathbf{n}$ ($\theta, \phi=0°$) has a recombination time ~550 ps, that is unchanged by the

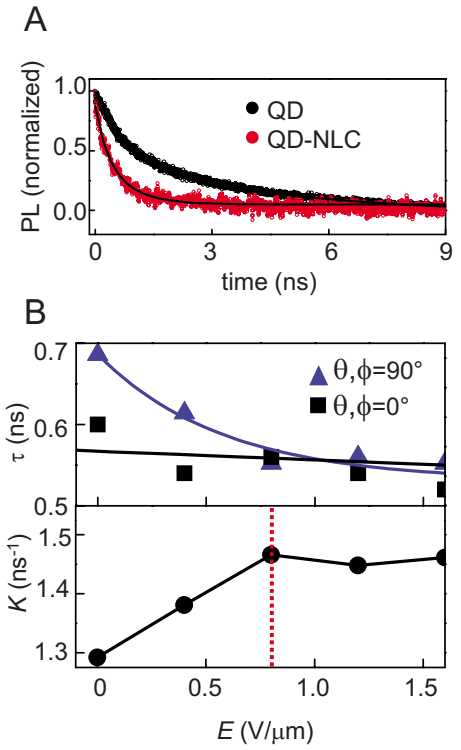

FIG. 3. (Color online) (a) Time-resolved PL for isolated QDs in toluene and in NLC matrix. (b) (Top) PL lifetime obtained from exponential fits to time-resolved traces for different $E \perp \mathbf{n}$ for QD-NLC sample, shown for the two collection geometries, $\phi=0°$ and 90° under copolarized conditions. (Bottom) Energy-transfer rate K can be enhanced by the application of E until 0.8 V/μm, which is almost equal to the threshold field for NLC realignment (indicated by the dotted red line).

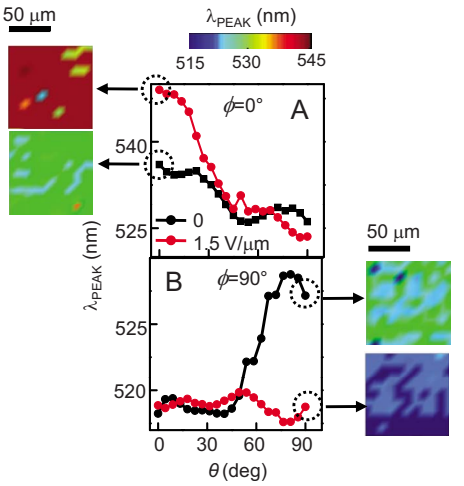

FIG. 4. (Color online) PL collected in (a) $\phi=0°(\perp E)$ and (b) $\phi=90°(\| E)$ collection geometries showing λ_{PEAK} varying with θ at $E=0$ and 1.5 V/μm. Spatial scans of λ_{PEAK} are shown beside the plots. These are performed over a representative 100 μm $\times$100 μm area of the sample at $E=0$ and 1.5 V/μm at excitation and polarization marked by circles. The color scheme used for all scans is represented by the color bar on top. Lines are guide to the eyes.

applied electric field The emission along $\theta, \phi=90°$ demonstrates a different trend where τ_{CQD} decreases from 700 to 550 ps with increasing E. We calculate an energy-transfer rate $K=1/\tau_{ET}$ from the equations above and find that it increases almost linearly by 15% before saturating at $E \sim 0.8$ V/μm, seen in Fig. 3(B) (bottom).

To better understand the electric field dependent optical properties exhibited in Figs. 2 and 3, we spectrally analyze the electric field induced intensity and polarization modulation. Figure 4 shows λ_{PEAK} of the emission spectra whose integrated intensity was mapped out in Fig. 2(C). Figure 4(A) [Fig. 4(B)] is a map of λ_{PEAK} as a function of θ for $\phi=0°$ (90°) at $E=0$ and 1.5 V/μm. At $E=0$, for both cases ($\theta, \phi=0°$ and $\theta, \phi=90°$), λ_{PEAK} lies in the range 525–530 nm. As θ increases from 0° to 90° we observe a blueshift for the emission collected along $\phi=0°$ while under the same conditions a redshift is seen for $\phi=90°$. Simply stated, under both copolarized conditions ($\theta=\phi$) the coupled QD assemblies that dominate the spectra are more strongly coupled than under contrapolarized conditions. This symmetry is broken with the application of the electric field. For the emission along $\phi=0°$, increasing E results in a spectral redshift, and at $E=1.5$ V/μm, the peak emission occurs at 548 nm. In contrast, the emission along $\phi=90°$ blueshifts with increasing E at $\theta=90°$.

In conjunction with the intensity profile in Fig. 2(A) and the dynamic results of Fig. 3(B), the above data allows a physical picture to emerge as follows: at $E=0$, most of the coupled QD structures are aligned along **n**, irrespective their size and coupling strength, and this causes the emission to be polarized preferentially along the x axis. But the polarization of the QD emission is only 0.62, implying that there are domains where the QD aggregates do not align along **n**. The QD structures in these regions do not follow the general alignment norm and contribute to the signal observed along $\phi=90°$ at $E=0$. What happens as E is increased is that it causes a physical reorientation of the smaller, or weaker, QD aggregates from alignment along x to y axis while leaving the orientation of the far redshifted strongly coupled aggregates unaltered. Inherently, the smaller aggregates have a higher population in the sample explaining why the intensity increases in absolute terms with their realignment. The larger aggregates on the other hand are fewer in number and their spectral signature shows up only when the external field E has rotated the smaller ones away from **n** to orient along the direction perpendicular to it. That the largest aggregates do not reorient with E is a surprising result but one that can be explained. The application of the electric field results in local reorientation of the NLC molecules. While the reorientation of the aggregates is energetically favored, their large size relative to the NLC molecules means that there has to be significant global rearrangement of the NLC matrix to accommodate the aggregate rotation. This means that the aggregate reorientation is kinetically limited with the barrier for reorientation growing rapidly with aggregate size. Thus we may anticipate that the smallest aggregates reorient with far more ease than the largest ones, in agreement with our results. This picture also ties in with the time-resolved data shown in Fig. 3. Along $\theta, \phi=0°$ the recombination is controlled by the long-wavelength aggregates from the very be-

ginning, irrespective of the applied E. At low E their spectral signature is muted by the presence of the large number of shorter clusters but the excitons migrate to these sites regardless and they dominate the dynamic signal. And as their orientation remains unaltered at high E, so does τ_{CQD}. Along the other direction although spectral emission blueshifts with E the recombination time decreases simply from an enhanced population increase due to the smaller aggregates lining up in larger numbers from the reorientation.

This size-selective reorientation is further clarified in the accompanying maps in Fig. 4. These show the spatial variation in λ_{PEAK} over the same 100 μm$\times$100 μm area of the sample under different excitation and collection geometries. At $\theta, \phi = 0°$ (top scans) with $E=0$ the emission is centered around 530 nm. At $E=1.5$ V/μm, $\lambda_{PEAK} > 540$ nm over the scanned area. For $\theta, \phi = 90°$ at $E=0$ the peak emission is in the region 520–525 nm but at $E=1.5$ V/μm it ranges between 515–520 nm over that same area. This results in spectral segregation of the coupled QDs based on their sizes causing the PL from the same spatial region in the sample to have different "colors" along the two polarization axes. Additionally, this effect is spatially homogenous over macroscopic regions. The reversibility of this field-induced alignment is not unambiguously established yet, but it is also worth noting that the emission with $E \neq 0$ is centered at 515 nm at the very least, still far redshifted from isolated QD emission. This, in addition to the fast excitonic recombination rate, definitely proves that the reorientation process does not destroy the interdot coupling and the application of E does provide an external nondestructive control to manipulate the landscape of these coupled QDs *in situ*.

Chemically synthesized QDs are very efficient absorbers with a particularly rich potential application in fourth generation hybrid photovoltaic devices. Currently, light harvesting efficiency in QD-based systems is critically low, often limited by the energetic disorder in ensembles. Our demonstration of postsynthesis external control over the electronic coupling of QDs is a possible corrective route toward enhancing this efficiency. Additionally, the spectrally selective spatial orientation of coupled QD nanoassemblies would offer a unique design for fast and directional energy transfer. The observations of these effects at room temperature under ambient conditions make our results all the more attractive for incorporation into the above devices.[22]

The authors would like to acknowledge support from NSF under Awards No. DMR-822171, No. CBET-0932404, and No. DMR-BMAT0852791, and from DOE under Award No. DE-FG02-04ER15502.

*sghosh@ucmerced.edu

[1] Q. Sun, Y. A. Wang, L. S. Li, D. Wang, T. Zhu, J. Xu, C. Yang, and Y. Li, Nat. Photonics **1**, 717 (2007).
[2] D. M. Willard, L. L. Carillo, J. Jung, and A. Van Orden, Nano Lett. **1**, 469 (2001).
[3] A. Imamoglu, D. D. Awschalom, G. Burkard, D. P. DiVincenzo, D. Loss, M. Sherwin, and A. Small, Phys. Rev. Lett. **83**, 4204 (1999).
[4] S. Kako, C. Santori, K. Hoshino, S. Gotzinger, Y. Yamamoto, and Y. Arakawa, Nature Mater. **5**, 887 (2006).
[5] M. Caruge, J. E. Halpert, V. Wood, V. Bulovi, and M. G. Bawendi, Nat. Photonics **2**, 247 (2008).
[6] E. Kikuchi, S. Kitada, A. Ohno, S. Aramaki, and S. Maenosono, Appl. Phys. Lett. **92**, 173307 (2008).
[7] M. Ouyang and D. D. Awschalom, Science **301**, 1074 (2003).
[8] J. A. Gupta, R. Knobel, N. Samarth, and D. D. Awschalom, Science **292**, 2458 (2001).
[9] S. A. Crooker, J. A. Hollingsworth, S. Tretiak, and V. I. Klimov, Phys. Rev. Lett. **89**, 186802 (2002).
[10] F. Levy, *Physics and Chemistry of Materials with Layered Structure* (Reidel, Holland, 1976).
[11] E. Mooser and M. Schluter, Nuovo Cimento Soc. Ital. Fis., B **18B**, 164 (1973).
[12] H. Tu, S. Yang, V. Chikan, and D. F. Kelley, J. Phys. Chem. B **108**, 4701 (2004).
[13] V. Chikan and D. F. Kelley, Nano Lett. **2**, 141 (2002).
[14] H. Tu, K. Mogyorosi, and D. F. Kelley, Phys. Rev. B **72**, 205306 (2005).
[15] E. O. Potma and D. A. Wiersma, J. Chem. Phys. **108**, 4894 (1998).
[16] H. Fidder, J. Knoester, and D. A. Wiersma, J. Chem. Phys. **98**, 6564 (1993).
[17] P. Jordan, P. Fromme, H. T. Witt, O. Klukas, W. Saenger, and N. Krau, Nature (London) **411**, 909 (2001).
[18] D. Zigmantas, Y.-Z. Ma, E. L. Read, and G. R. Fleming, in *Biophysical Techniques in Photosynthesis II*, edited by T. J. Aartsma and J. Matysik (Springer, Dordrecht, 2008), pp. 201–222.
[19] J. Shao, H. Mirafzal, J. R. Petker, J. L. S. Cosio, D. F. Kelley, and T. Ye, J. Phys. Chem. C **113**, 19102 (2009).
[20] L. C. T. Shoute and D. F. Kelley, J. Phys. Chem. C **111**, 10233 (2007).
[21] C. R. Kagan, C. B. Murray, M. Nirmal, and M. G. Bawendi, Phys. Rev. Lett. **76**, 1517 (1996).
[22] L. S. Hirst, J. Kirchhoff, R. Inman, and S. Ghosh, Proc. SPIE **7618**, 76180F1-7 (2010).